



### Special Section:

The COVID-19 pandemic: linking health, society and environment

### Key Points:

- COVID-19 lockdown-related reductions in on-road NO<sub>x</sub> emissions tracked by TROPOspheric Monitoring Instrument (TROPOMI) tropospheric nitrogen dioxide column observations
- On-road NO<sub>x</sub> emissions continued to be ~20% below normal through December 2020 in parts of the US even after lockdowns were lifted in the US
- Increase in the unemployment rate in the second quarter of 2020 correlated negatively with TROPOMI tropospheric nitrogen dioxide column amount

### Supporting Information:

Supporting Information may be found in the online version of this article.

### Correspondence to:

S. Kondragunta,  
Shobha.Kondragunta@noaa.gov

### Citation:

Kondragunta, S., Wei, Z., McDonald, B. C., Goldberg, D. L., & Tong, D. Q. (2021). COVID-19 induced fingerprints of a new normal urban air quality in the United States. *Journal of Geophysical Research: Atmospheres*, 126, e2021JD034797. <https://doi.org/10.1029/2021JD034797>

Received 21 FEB 2021

Accepted 8 AUG 2021

### Author Contributions:

**Data curation:** B. C. McDonald

© 2021 The Authors. This article has been contributed to by US Government employees and their work is in the public domain in the USA. This is an open access article under the terms of the Creative Commons Attribution-NonCommercial-NoDerivs License, which permits use and distribution in any medium, provided the original work is properly cited, the use is non-commercial and no modifications or adaptations are made.

## COVID-19 Induced Fingerprints of a New Normal Urban Air Quality in the United States

S. Kondragunta<sup>1</sup> , Z. Wei<sup>2</sup>, B. C. McDonald<sup>3</sup>, D. L. Goldberg<sup>4</sup>, and D. Q. Tong<sup>5</sup>

<sup>1</sup>NOAA NESDIS Center for Satellite Applications and Research, College Park, MD, USA, <sup>2</sup>IM Systems Group, College Park, MD, USA, <sup>3</sup>NOAA Chemical Systems Laboratory, Boulder, CO, USA, <sup>4</sup>Milken School of Public Health, George Washington University, Washington, DC, USA, <sup>5</sup>Department of Atmospheric, Oceanic, and Earth Sciences, George Mason University, Fairfax, VA, USA

**Abstract** Most countries around the world, including the United States, took actions to control COVID-19 spread that led to an abrupt shift in human activity. On-road NO<sub>x</sub> emissions from light and heavy-duty vehicles decreased by 9%–19% between February and March at the onset of the lockdown period in the middle of March in most of the US; between March and April, the on-road NO<sub>x</sub> emissions dropped further by 8%–31% when lockdown measures were most stringent. These precipitous drops in NO<sub>x</sub> emissions correlated well ( $r = 0.75$ ) with tropospheric NO<sub>2</sub> column amount observed by the Sentinel 5 Precursor TROPOspheric Monitoring Instrument (S5P TROPOMI). Furthermore, the changes in TROPOMI tropospheric NO<sub>2</sub> column amount across continental US between 2020 and 2019 correlated well with the changes in on-road NO<sub>x</sub> emissions ( $r = 0.68$ ) but correlated weakly with changes in emissions from the power plants ( $r = 0.35$ ). At the height of lockdown-related unemployment in the second quarter of 2020, the tropospheric NO<sub>2</sub> column values decreased at the rate of 0.8  $\mu\text{moles/m}^2$  per unit percentage increase in the unemployment rate. Despite the lifting of lockdown measures, parts of the US continued to have ~20% below normal on-road NO<sub>x</sub> emissions. To achieve this new normal urban air quality in the US, continuing remote work policies that do not impede economic growth may become one of the many options.

**Plain Language Summary** This study documents the different phases of COVID-19 lockdown in 2020 and how traffic emissions changed accordingly across the US, particularly in five different cities, namely Los Angeles, San Francisco, San Joaquin Valley, New York City, and Atlanta. Analysis of data for these cities from measurements on the ground and satellites indicate that a downturn in the economy and telework policies reduced the number of cars and trucks on the road in March and April due to which air quality got better. The recovery of traffic emissions after the lockdowns was lifted was slow and below normal emissions were observed even at the end of 2020. While the cities in the east reached near normal levels, the west coast showed below normal traffic emissions. The air quality in 2020 provided a window into the future as to how improvements can be achieved.

## 1. Introduction

As the 2019 novel Corona virus (COVID-19) spread from China to other parts of the world, various countries imposed lockdown measures one by one. Reports of improved air quality from ground and satellite observations of aerosol optical depth (AOD) and nitrogen dioxide (NO<sub>2</sub>) soon followed in the media as documented by Kondragunta et al. (2020). The precipitous drops seen in the tropospheric vertical column NO<sub>2</sub> (trop-NO<sub>2</sub> here onward) measured by the Sentinel 5P TROPOspheric Monitoring Instrument (TROPOMI) were substantial, especially during the strict lockdown period for each country (Gkatzelis et al., 2021). Goldberg et al. (2020) reported that in the United States (US), tropNO<sub>2</sub> decreased by 9.2%–45% in 26 cities from March 15 to April 30, 2020 compared to the same period in 2019; these reported reductions account for the influence of the weather. Other researchers reported similar findings, mainly reductions of tropNO<sub>2</sub> attributed to reductions in traffic emissions both in the US and across the globe in major urban areas of Europe, India, and China (Bauwens et al., 2020; Keller et al., 2020; Naeger & Murphy, 2020; Straka et al., 2021; Vadrevu et al., 2020; Zhang et al., 2021; Zheng et al., 2020). For example, in Washington D.C., the average distance traveled by people dropped by 60% between February and April when restrictions were fully in place (Straka et al., 2021). This sudden drop in tropNO<sub>2</sub> in major metropolitan areas where the transportation source

**Formal analysis:** S. Kondragunta, Z. Wei, B. C. McDonald  
**Visualization:** Z. Wei  
**Writing – review & editing:** S. Kondragunta, D. L. Goldberg, D. Q. Tong

sector for  $\text{NO}_x$  ( $\text{NO} + \text{NO}_2$ ) is strong is due to reduced traffic on top of an already observed general decreasing trend in  $\text{NO}_x$  emissions. According to Lamsal et al. (2015), trop $\text{NO}_2$  observed by the Ozone Monitoring Instrument (OMI) showed a decreasing trend with an overall decrease of 28% between 2005 and 2013. These reductions are consistent with  $\text{NO}_x$  emission reductions from major power plants in the US due to the Clean Air Interstate Rule and Cross State Air Pollution Rule. The  $\text{NO}_x$  emissions continued to drop as more and more power plants switched to natural gas or began to rely on clean coal (de Gouw et al., 2014).

Nitrogen dioxide is released during the combustion of fossil fuels and is a precursor for both ozone and particulate matter, primary components of photochemical smog. Whether it enhances or decreases ozone production is dependent on a given region being  $\text{NO}_x$  saturated or volatile organic compound (VOC) saturated, due to the inherent nonlinearity of ozone photochemistry (Kroll et al., 2020; Mazuuca et al., 2016). The two main sources of  $\text{NO}_2$  in the US are the energy sector and the transportation sector according to the 2014 Community Emissions Data System (Hoesly et al., 2018). A study by Zheng et al. (2020) analyzed the reductions in trace gas and aerosol concentrations in China during the lockdown and found that the most significant drop in aerosols was for nitrate aerosol. For the period corresponding to the lockdown in China, from January 23 to February 22, 2020, mean nitrate aerosol concentration was  $14.1 \mu\text{g}/\text{m}^3$ ; for the same period in 2019, the concentration was  $23.8 \mu\text{g}/\text{m}^3$ . This 41% reduction is corroborated by reductions in  $\text{NO}_2$  observed by TROPOMI (Bauwens et al., 2020).

Though  $\text{NO}_2$  is considered important due to its ozone and aerosol-producing potential, it has harmful human health impacts when inhaled. Achakulwisut et al. (2019) showed that 64% of 4 million pediatric asthma cases each year are due to exposure to  $\text{NO}_2$ . It should be noted though that  $\text{NO}_2$  was used as a proxy for traffic-related pollution. The World Health Organization standard for  $\text{NO}_2$  is an annual average of 21 parts per billion and for the US, it is 53 parts per billion. The authors do note that daily exposure to  $\text{NO}_2$  can vary from annual averages, and traffic pollution is usually a mixture of precursor gases, primary particulates, and photochemically formed ozone and aerosols. Nevertheless, when countries went into lockdown, the most noticeable indication of a reduction in traffic-related pollution is trop $\text{NO}_2$  in urban areas observed by TROPOMI, lending support to the assumption that  $\text{NO}_2$  is a good proxy for traffic-related pollution. The COVID-19 lockdown measures disproportionately impacted traffic more than industrial operations.

We analyzed TROPOMI trop $\text{NO}_2$  and Suomi National Polar-orbiting Partnership Visible Infrared Imaging Radiometer Suite (Suomi NPP VIIRS) AOD data in conjunction with on-road  $\text{NO}_x$  emission data,  $\text{NO}_x$  emissions from power plants, and unemployment rates where available. The goal of this study is to examine the trends in on-road and power plant emissions for five different locations (four urban areas and one rural area) to answer the questions: (a) are changes in  $\text{NO}_x$  emissions during the lockdown detectable in TROPOMI trop $\text{NO}_2$  data, (b) are the economic indicators consistent with emissions changes, and (c) did the trends reverse with the lifting of lockdown measures in the major metro areas. These questions are answered with spatial and temporal analysis of ground-based observations and satellite data, relating indicators of human activity during and prior to COVID-19 lockdown with air quality, and examining if a new normal urban air quality can be achieved with novel policies.

## 2. Methods

### 2.1. Sentinel 5P TROPOMI $\text{NO}_2$

The TROPOMI  $\text{NO}_2$  algorithm is based on the Differential Optical Absorption Spectroscopy technique that involves fitting the spectra in the  $\text{NO}_2$  absorption region between 405 and 465 nm using known laboratory-measured reference absorption spectra. The Sentinel 5P flies in formation with Suomi NPP. Though some Sentinel 5P trace gas algorithm retrievals depend on the VIIRS cloud mask, the  $\text{NO}_2$  algorithm relies on cloud retrievals using its oxygen A-band absorption (van Geffen et al., 2019). The cloud fraction and effective pressure are used in air mass factor calculation for partially cloudy pixels. There is an indication that the cloud algorithm is likely conservatively masking out good  $\text{NO}_2$  retrievals according to a validation study conducted by Judd et al. (2020). Though Judd et al. (2020) used data with quality flag equals to unity, we used the quality flag value (0.75) recommended by the  $\text{NO}_2$  algorithm theoretical basis document (van Geffen et al., 2019). Only data with quality flag  $>0.75$  were used as this quality flag setting ensures that cloudy retrievals or retrievals with snow/ice covered pixels are screened out. The TROPOMI Level 2 product

file consists of pixel level ( $3.5 \times 5.6$  km)  $\text{NO}_2$  tropospheric column amount, which we used in this study. The  $\text{NO}_2$  algorithm retrieves total column  $\text{NO}_2$  and separates the stratosphere from troposphere using chemical transport model predicted stratospheric  $\text{NO}_2$  analysis fields (van Geffen et al., 2019). The expected accuracy of the tropospheric  $\text{NO}_2$  column for polluted regions with high  $\text{NO}_2$  values is  $\sim 25\%$ , and independent validation efforts using ground-based spectrometers such as Pandora have confirmed that trop $\text{NO}_2$  is generally underestimated, especially in polluted regions and that significant sources of errors come from coarser resolution a priori profiles used in the retrieval algorithm (Chan et al., 2020). Comparisons of TROPOMI trop $\text{NO}_2$  column with Pandora ground station retrievals of tropospheric  $\text{NO}_2$  column in Helsinki showed that mean relative difference is  $-28.2\% \pm 4.8\%$  (Ialongo et al., 2020). Similar comparisons between Pandora ground station retrievals and TROPOMI trop $\text{NO}_2$  in Canada for urban (Toronto) and rural (Egbert) stations show that TROPOMI trop $\text{NO}_2$  has a  $-23\%$  to  $-25\%$  bias for polluted regions and a  $7\%-11\%$  high bias in the rural region (Zhao et al., 2020). Sources of error in TROPOMI trop $\text{NO}_2$  include altitude-dependent air mass factors, stratosphere-troposphere separation of  $\text{NO}_2$ , a priori  $\text{NO}_2$  profile and shape, surface albedo climatology, and calibration errors as a function of view angle (Chan et al., 2020; Ialongo et al., 2020; Judd et al., 2020; van Geffen et al., 2019; Zhao et al., 2020). Judd et al. (2020) showed that the TROPOMI trop $\text{NO}_2$  validation carried out during the Long Island Sound Tropospheric Ozone Study experiment showed that the retrievals have a bias of  $-33\%$  and  $-19\%$  versus Pandora and airborne spectrometer retrievals, respectively. The biases improve to  $-19\%$  and  $-7\%$  when the TROPOMI  $\text{NO}_2$  algorithm is run with a priori profiles from a regional air quality model indicating that retrievals are very sensitive to a priori profiles. One aspect that is not fully explored by Judd et al. (2020) is the influence of aerosols on air mass factor calculations. Research on aerosol impact on air mass factors indicates that the effect of aerosols on  $\text{NO}_2$  retrieval can vary depending on aerosol type (absorbing or scattering), amount, and vertical location (is aerosol mixed in with  $\text{NO}_2$  in the boundary layer or is the aerosol layer detached from  $\text{NO}_2$  layer) in the atmospheric column (Judd et al., 2020; Lin et al., 2014; Liu et al., 2020; Tack et al., 2019).

The Level 2 TROPOMI  $\text{NO}_2$  data were downloaded from the European Space Agency datahub (<https://s5phub.copernicus.eu/dhus/#/home>). The data for January–February 2020 are considered Business as Usual (BAU), the data for 15 March to 30 April 2020 are considered the lockdown period, and the data for 1 May–November 2020 are considered as representing the post-lockdown period.

The TROPOMI  $\text{NO}_2$  data are available only from mid-2018 to the present. We removed the seasonality in trop $\text{NO}_2$  data in two simple ways: by simply taking the difference between 2019 and 2020 for the same month so the sun-satellite geometries and weather conditions are similar barring any unusual interannual variabilities and by doing double differencing as described in Section 3.1.

## 2.2. On-Road $\text{NO}_x$ Emissions

The on-road emissions are obtained using the Fuel-based Inventory of Vehicle Emissions (FIVE) where vehicular activity is estimated using taxable fuel sales for gasoline and diesel fuel reported at a state-level and downscaled to the urban scale using light- and heavy-duty vehicle traffic count data (McDonald et al., 2014). Once the fuel use is mapped,  $\text{NO}_x$  emissions are estimated using fuel-based emission factors (in g/kg fuel) based on roadside measurements or tunnel studies (Hassler et al., 2016; McDonald et al., 2012, McDonald, McKeen, et al., 2018). The emission factors are calculated separately for light-duty gasoline vehicles and heavy-duty diesel trucks. The FIVE methodology was developed to derive traffic emissions to study their impact on air quality (Kim et al., 2016; McDonald, McKeen, et al., 2018), but in the case of 2020, the fuel-based methods provide evidence for quantifying the impact of reduced human activity during the lockdown period on air pollutant emissions (e.g.,  $\text{NO}_x$ ).

Here, we downscale on-road gasoline and diesel fuel sales following McDonald et al. (2014) for our 2019 base year, which is treated as the BAU case. We have chosen to focus on four US urban areas where real-time traffic counting data are publicly available, including the South Coast air basin (Los Angeles county, Orange county, and portions of Riverside and San Bernardino counties), San Francisco Bay Area (Marin, Sonoma, Napa, Solano, Contra Costa, Alameda, Santa Clara, San Mateo, and San Francisco counties), New York City (Richmond, New York, Kings, Queens, and Bronx counties), and the Atlanta metropolitan region (Cherokee, Clayton, Cobb, Coweta, Dekalb, Douglas, Forsyth, Fulton, Gwinnett, Henry, Rockdale, and Spalding counties). We also include one rural region for contrast, the San Joaquin Valley in California (Fresno, Kern,

Kings, Madera, Merced, San Joaquin, Stanislaus, and Tulare counties. For the BAU case, we account for typical seasonal and day-of-week activity patterns of light- and heavy-duty vehicles separately. For the COVID-19 case, we scale the January BAU emissions case with real-time light- and heavy-duty vehicle traffic counting data for the year 2020, which are described in Harkins et al. (2021). Light-duty vehicle counts are used to project on-road gasoline emissions and heavy-duty truck counts for on-road diesel emissions during the pandemic.

To estimate  $\text{NO}_x$  emissions, the FIVE  $\text{NO}_x$  emission factors have been updated to 2019 based on the regression analyses of roadway studies (Hassler et al., 2016; McDonald et al., 2012, McDonald, McKeen, et al., 2018), and we use a value of running exhaust emission factors of  $1.7 \pm 2 \text{ g NO}_x/\text{kg fuel}$  and  $12.4 \pm 1.9 \text{ g NO}_x/\text{kg fuel}$  for on-road gasoline and diesel engines, respectively. Cold-start emissions are scaled relative to running exhaust emissions based on the US Environmental Protection Agency (EPA) MOVES2014 model (EPA, 2015). We use the 2019  $\text{NO}_x$  emission factor for both the BAU- and COVID-19-adjusted cases. Thus, the differences in the BAU and COVID-19 cases are only due to changes in traffic activity. We use the same emission factor for 2019 and 2020 because past studies have shown during the 2008 Great Recession the turnover of the vehicle fleet and corresponding reductions in emission factors are slower (Bishop & Stedman, 2014). Total on-road  $\text{NO}_x$  emissions are the sum of emission estimates for light-duty vehicles and heavy-duty trucks. The off-road mobile source emissions are not included in the data set. In cities, on-road transportation accounts for as much as 75% of the  $\text{NO}_x$  emissions (Kim et al., 2016) and is a critical emissions sector to quantify.

Uncertainties in FIVE on-road emission estimates arise from non-taxable fuel sales associated with off-road machinery, and from mismatches where fuel is sold and where driving occurs, though diesel fuel sales reports are adjusted based on where long-haul trucking occurs (McDonald et al., 2014). However, the main source of uncertainty is the accuracy of fuel-based emission factors used to calculate co-emitted air pollutant species (McDonald, McKeen, et al., 2018). The underlying traffic counting data are available at hourly time resolution; however, here we have averaged the data to daily averages. Jiang et al. (2018) report the uncertainty in fuel sales (3%–5%) and  $\text{NO}_x$  emission factors (15%–17%) for on-road transportation.

### 2.3. Power Plant $\text{NO}_x$ Emissions

The daily power plant  $\text{NO}_x$  emissions were obtained from the US EPA Continuous Emissions Monitoring System (<https://www.epa.gov/airmarkets>), and the energy generation/consumption statistics were obtained from the Energy Information Administration ([eia.gov](http://eia.doe.gov)). Unlike the traffic emissions, power plant emissions did not change much during the lockdown. Power generation from fossil fuels dropped from 38,332 Gwh in March to 29,872 Gwh in April and rebounded to pre-pandemic levels by June. The total  $\text{NO}_x$  emissions in the US from power plants dropped from 54,531 tons in March to 44,016 tons in April, a 19% decrease. This may seem like a big drop in production but the absolute values are quite small. For example,  $\text{NO}_x$  emissions from power plants within the 75 km of Los Angeles emitted only 20 tons in March 2020. For January to July, nationally, total  $\text{NO}_x$  emissions from power plants were 0.8 and 0.67 million metric tons in 2019 and 2020, respectively. This is a 16% reduction compared to 50% reduction in on-road emissions, for the same months between 2019 and 2020.

In contrast, on-road emissions from vehicles in the Los Angeles area alone emitted nearly 5,367 tons of  $\text{NO}_x$ . Power plant  $\text{NO}_x$  emissions in the US have decreased substantially over the last two decades; they dropped by 86% between 1990 and 2019. This is due to the shift from fossil fuels to other alternate energy sources for power generation. For example, the use of coal as a source of electricity generation went down from 51% in 2001 to 23% in 2019, while the natural gas as a source increased from 17% in 2001 to 38% in 2019. In our analysis of  $\text{NO}_x$  emissions from on-road traffic and power plants for the six locations of interest, we considered only the power plants within 75 km radius of the center of the city location being analyzed.

### 2.4. Suomi National Polar-Orbiting Partnership Visible Infrared Imaging Radiometer Suite (SNPP VIIRS)

NOAA currently has two VIIRS instruments in orbit - one on Suomi NPP launched on October 28, 2011 and one on NOAA-20 launched on November 18, 2017. The two VIIRS instruments continuously observe the Earth with a 50-min time difference and provide AOD retrievals for cloud/snow-free scenes during the

sunlit portion of the day. The VIIRS instruments have 22 bands with 16 of the bands in the visible to long-wave infrared at moderate resolution (750 m), five bands at imager resolution (375 m) covering 0.64, 0.865, 1.6, 3.74, and 11.45  $\mu\text{m}$ , and one broad Day-Night Band centered at 0.7  $\mu\text{m}$ . The NOAA AOD algorithm over the ocean is based on the Moderate Imaging Spectroradiometer (MODIS) heritage and over the land, the algorithm derives AOD for both dark targets as well as bright surfaces (Laszlo & Liu, 2016; Levy et al., 2007; Huang et al., 2016; Zhang et al., 2016). For this study, we used the Suomi NPP VIIRS AOD because Suomi NPP flies in formation with S5P TROPOMI with a local equator crossing time of 1:30 p.m. and less than three minutes difference in overpass time. The Suomi NPP VIIRS AOD product has been extensively validated by comparing it to Aerosol Robotic Network (AERONET) AODs and the VIIRS 550 nm AOD is shown to have a global bias of  $-0.046 \pm 0.097$  for AODs over land less than 0.1 and for AODs between 0.1 and 0.8, the bias is  $-0.194 \pm 0.322$ . In the US, for VIIRS AODs ranging between 0.1 and 0.8, the bias is  $-0.008 \pm 0.089$  and for AODs greater than 0.8, the bias is about  $0.068 \pm 0.552$  (Zhang & Kondragunta, 2021). For the analysis of AOD data in this study, we remapped the high quality (Quality Flag equals 0) 750 m resolution AOD retrievals to  $0.05^\circ \times 0.05^\circ$  resolution with a criterion that for a grid to have a mean AOD value, there should be a minimum of 20% 750 m pixels with high-quality AODs.

## 2.5. Unemployment Rate

The civilian labor force and unemployment estimates for metropolitan areas were obtained through the Local Area Unemployment Statistics (LAUS) provided by the Bureau of Labor Statistics ([bls.gov](https://www.bls.gov)). The LAUS program is a federal-state cooperative effort in which monthly estimates of total employment and unemployment are prepared for over 7,500 areas including metropolitan areas. The seasonal adjustments are carried out by the Current Employment Statistics State and Area program (CES) using the statistical technique Signal Extraction in Auto Regressive Integrated Moving Average Time Series (SEATS). These data sets are smoothed using a Reproducing Kernel Hilbert Space filter after seasonal adjustment. The details of the data collection, processing and release can be found at <https://www.bls.gov/lau/laumthd.htm>. The data used in this study are for January–November 2020. To compare the  $\text{NO}_2$  variation in metropolitan areas, the TROPOMI trop $\text{NO}_2$  column amounts were averaged inside each metropolitan area. The 1:500,000 polygon shape files were used to test if a TROPOMI pixel is inside or outside a metropolitan area. The shape files are from US Census Bureau (<https://www.census.gov/geographies/mapping-files/time-series/geo/cartographic-boundary.html>).

## 2.6. Matchup Criteria

The  $\text{NO}_2$  data were matched to the on-road mobile emissions data for statistical and trend analysis with certain criteria. Prior to generating the matchups, rotated wind analysis was carried out on the original pixel level data. It is important to do this when sampling the satellite data because  $\text{NO}_2$  concentrations accumulate in the cities when wind speed is low and disperse away from the city when wind speed is high. The satellite data are observed once a day in the midafternoon, whereas on-road mobile emissions represent daily values. To have representative sampling, it is common to rotate the satellite pixel-level data in the direction of the wind (Fioletov et al., 2015; Goldberg et al., 2019; Lorente et al., 2019; Zhao et al., 2020). We used the European Center for Medium range Weather Forecast (ECMWF) Re-Analysis (ERA5) 30-km resolution global wind fields (Hersbach et al., 2020). To do the wind rotation, each TROPOMI pixel was collocated to ERA5 with tri-linear interpolation method in both temporal and horizontal directions. The wind profiles were merged to the location of the TROPOMI pixel center. The east-west (U) and north-south (V) wind speed components were averaged through the vertical distribution within the bottom 100 hPa, approximated to be within the boundary layer. Then, each TROPOMI pixel was rotated and aligned with the average wind direction from the city center. The rotated pixels are gridded with  $5 \times 5$  km resolution to generate monthly mean values for correlation analysis with on-road  $\text{NO}_x$  emissions.

Once the pixels are rotated, they are sampled for 100 km in the downwind direction, 50 km in the upwind direction, and the crosswind direction. This way, the elevated concentrations of  $\text{NO}_2$  moving away from the city in the downwind direction are captured. Figure 1a shows an example of the TROPOMI trop $\text{NO}_2$  with Los Angeles as the focus. The trop $\text{NO}_2$  data shown are monthly mean values for January 2020 remapped to a fixed grid. The black rectangle shows the area of interest over Los Angeles that we want to compare with

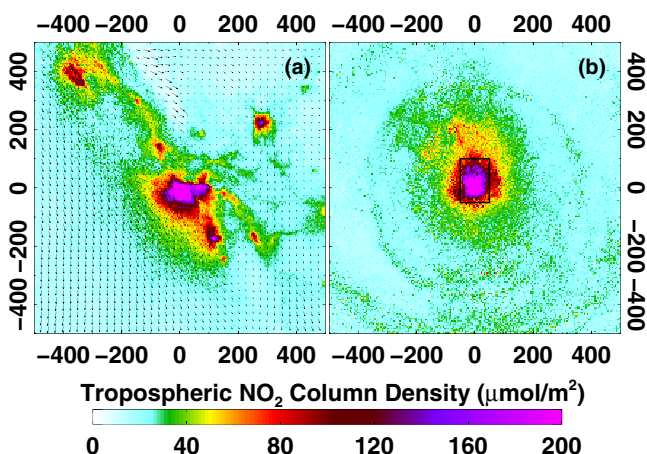


**Figure 1.** Sentinel 5P TROPOMI monthly mean tropNO<sub>2</sub> column amount (or density) for January 2020 for Los Angeles. (a) Original pixel level data remapped to  $5 \times 5 \text{ km}$  resolution and averaged for the month. The monthly mean ERA5 wind vectors are overlaid on the tropNO<sub>2</sub> map to indicate the wind direction. (b) Remapped tropNO<sub>2</sub> data grids rotated in the direction of the wind using ERA5 wind fields. The downwind direction is toward North (zero on the axis). For the monthly mean to be computed, we used a criterion that at least 25% of the days in a month should have retrievals. The black rectangle defines the area for which tropNO<sub>2</sub> data are averaged.

ing the height of the COVID-19 pandemic in different parts of the world and in the US. To remove the seasonality from the signal, researchers in these studies have adopted different approaches including the use of numerical models to simulate the seasonality (e.g., Goldberg et al., 2020; Liu et al., 2020; Silver et al., 2020). Seasonality should be accounted for because in the northern hemisphere winter months, tropNO<sub>2</sub> amounts are higher than in summer months; as a result, during the transition from winter to summer, tropNO<sub>2</sub> amounts are higher in February than in March. In our study, we used a double-differencing technique to account for seasonality. Consistent with Goldberg et al. (2020), we used 1 January to 29 February 2020 as the pre-lockdown period and 15 March to 30 April as the lockdown period. The difference in mean tropNO<sub>2</sub> between lockdown and pre-lockdown is referred to as 2020 $\Delta\text{NO}_2$ . For the same two corresponding periods in 2019, the difference in mean tropNO<sub>2</sub> is referred to as 2019 $\Delta\text{NO}_2$ . Then, the difference of 2019 $\Delta\text{NO}_2$  and 2020 $\Delta\text{NO}_2$  was computed to tease out the changes in tropNO<sub>2</sub> due to reductions in emissions during the lockdown ( $\Delta\text{tropNO}_2$ ). It should be noted though that the double differencing only removes the seasonality and does not fully account for differences in meteorological events such as precipitation or anomalously cold or hot conditions in one year versus the other but on a monthly time scale they are minimized.

Figures 2a and 2b show 2019 $\Delta\text{NO}_2$  and 2020 $\Delta\text{NO}_2$ , which include changes due to seasonality and any changes due to emissions either from natural sources such as fires or from anthropogenic urban/industrial sources. Figure 2c shows  $\Delta\text{tropNO}_2$  for the CONUS due to just changes in emissions between the pre-lockdown and lockdown periods in 2020 with the seasonality removed. Comparing Figures 2a and 2b, one can deduce that reductions in tropNO<sub>2</sub> between pre-lockdown and lockdown are much stronger in 2020 compared to 2019. However, the double difference plot in Figure 2c shows how much of that reduction seen in 2020 $\Delta\text{NO}_2$  (Figure 2b) is due to changes in emissions. The tropNO<sub>2</sub> changes are smaller in Figure 2c than in Figure 2b, both in magnitude as well as spatial extent of the reductions. Given that TROPOMI tropNO<sub>2</sub> precision is  $1 \times 10^{15} \text{ molecules/cm}^2$  or  $16.6 \mu\text{moles}/\text{m}^2$  and the mean background tropNO<sub>2</sub> for 2019 and 2020 is about  $16 \mu\text{moles}/\text{m}^2$  according to our estimates using Silvern et al. (2019) method, we subtracted  $16 \mu\text{moles}/\text{m}^2$  from tropNO<sub>2</sub> data in 2019 and 2020 before applying the double difference method. We also colored the values between  $-5$  and  $+5 \mu\text{moles}/\text{m}^2$  white.

The lockdown measures in most states in the US began in the middle of March 2020. The first state to institute stay-at-home measures was California on 19 March and the last state was Missouri on 6 April. The

on-road emissions. The ERA5 wind vectors are plotted on the tropNO<sub>2</sub> map to show wind direction. To do the wind rotation, daily tropNO<sub>2</sub> pixel level data are first remapped to a  $5 \times 5 \text{ km}$  fixed grid resolution. The grids are then rotated to align with the wind direction with downwind direction pointing North (Figure 1b). The daily rotated grid values of tropNO<sub>2</sub> in  $5 \times 5 \text{ km}$  are averaged over a month to generate a monthly mean. The monthly mean values can vary quite a bit depending on missing data due to screening for the high-quality data as well as cloud cover. In a given month, the number of pixels with valid retrievals for a city can vary from 2% to 100% depending on cloud and snow cover; the mean values vary depending on the location of the missing values, if they are in the center of the city where tropNO<sub>2</sub> is usually high or on the edges of the city where tropNO<sub>2</sub> values can be low depending on wind speed and direction. In our analysis for this study, prior to computing the monthly mean, the criterion we employed is that on a given day, there should be a minimum of 25% of pixels in a region selected for matchups of satellite data should have valid retrievals. The 25% threshold is a reasonable compromise because any value higher than that will reduce the sample size (number of days included in the monthly mean).

### 3. Results

#### 3.1. Deseasonalizing TropNO<sub>2</sub> Data

As already shown by many research studies, the global tropNO<sub>2</sub> column amounts dropped in coincidence with partial or complete lockdowns during the height of the COVID-19 pandemic in different parts of the world and in the US. To remove the seasonality from the signal, researchers in these studies have adopted different approaches including the use of numerical models to simulate the seasonality (e.g., Goldberg et al., 2020; Liu et al., 2020; Silver et al., 2020).

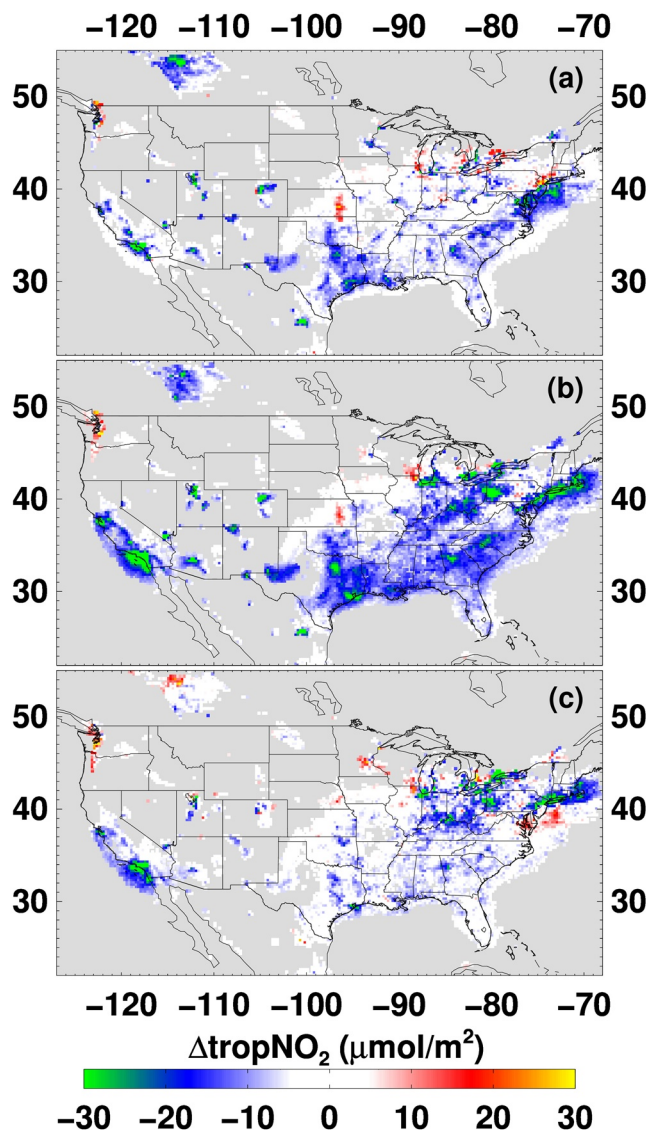


**Figure 2.**  $\text{tropNO}_2$  changes between pre-lockdown period (January to February) and lockdown period (15 March to 30 April) for (a)  $2019\Delta\text{NO}_2$ , (b)  $2020\Delta\text{NO}_2$ , and (c) the difference between  $2020\Delta\text{NO}_2$  and  $2019\Delta\text{NO}_2$ . The double differencing is expected to minimize the seasonal differences and provide a realistic estimate of change in  $\text{tropNO}_2$  due to emissions changes.

observations of  $\text{NO}_2$ , long-term observations of  $\text{tropNO}_2$  from OMI, TROPOMI  $\text{tropNO}_2$ , and the Goddard Earth Observing System Chemistry model, Qu et al. (2021) showed how the use of satellite  $\text{tropNO}_2$  data in interpreting changes in  $\text{NO}_x$  emissions can be complicated by background  $\text{tropNO}_2$ .

### 3.2. On-Road $\text{NO}_x$ Emissions and $\text{TropNO}_2$

Focusing on the regions of interest with on-road  $\text{NO}_x$  emissions available for this study, we calculated reductions in  $\text{tropNO}_2$  for Los Angeles, Atlanta, San Francisco, San Joaquin Valley, and New York City. We focus on the four cities from different regions of the country where daily traffic counting data are publicly available in real time. We also include the San Joaquin Valley as a rural region with available traffic counting data to compare with the urban areas. Based on real-time traffic counting data sets in each region, Table 2

cities/regions with worse traffic-related ozone pollution levels based on the monitoring data from 2016 to 2018 compiled by the American Lung Association and the duration for which they were in a lockdown are shown in Table 1. For regions that fall into different states (e.g., Washington-Baltimore-Arlington), the dates for the state that had the longest duration of lockdown are listed in the table. Most states were in a lockdown mode only for one to two months and given the varying nature of the lockdown in different parts of the country, we treated 15 March and 30 April as lockdown months. As shown in Figure 2a,  $2019\Delta\text{NO}_2$  is positive in some areas and negative in some areas, whereas in 2020 (Figure 2b), large negative values (reductions) are observed in most of the CONUS except in the Great Plains region and the Pacific Northwest. These reduced  $\text{tropNO}_2$  amounts are attributed to reduced emissions due to lockdowns. Changes in the rural areas (either positive or negative) of the US could be due to the changes to natural sources such as soil and lightning  $\text{NO}_x$  emissions or due to meteorological differences that the double differencing technique did not account for (Qu et al., 2021).

Liu et al. (2021) used NASA global photochemical model simulations to study how long the  $\text{tropNO}_2$  data need to be averaged to minimize the influence of meteorological variability. They simulated January 2019 to December 2020 by keeping the  $\text{NO}_x$  emissions the same between the two years and found that averaging the data over 31 days for the US leads to differences in  $\text{tropNO}_2$  between 2019 and 2020 less than 10%. Our double differencing was done with  $\text{tropNO}_2$  data averaged over 1.5 months, which should substantially minimize the differences in meteorology.

We tested the robustness of the double differencing technique in other ways. We repeated the analysis for a longer period and found that our conclusions did not change. Setting the pre-lockdown period as 1 January to 15 March and the lockdown period as 16 March to 30 May, we found that  $\text{tropNO}_2$  decreases are consistent with those shown in Figures 2a–2c (Figures S1a–S1c). We also applied scaling factors to account for seasonality and meteorological variability developed by Goldberg et al. (2020). These scaling factors normalize  $\text{tropNO}_2$  data to conditions of a typical week day based on TROPOMI  $\text{tropNO}_2$  data from 2018 to 2019, based on sun angle, wind speed, wind-direction, and day-of-week. Figure S2 shows this analysis using the normalized  $\text{tropNO}_2$  to investigate  $\text{NO}_x$  trends; it shows reductions in  $\text{tropNO}_2$  for different cities during the lockdown period that are consistent with the double differencing analysis.

We investigated the likely increase in background  $\text{tropNO}_2$  in 2020 compared to 2019 and found that it increased by 14.5% in the Pacific Northwest complicating the impact of emission reductions on  $\text{tropNO}_2$ . This is consistent with the analysis reported by Qu et al. (2021). Using surface

**Table 1**

*Ranking of Cities for Ozone Pollution and Their Lockdown Periods*

City/Region	Ozone pollution ranking	Lockdown start date	Lockdown end date
Los Angeles-Long Beach, CA	1	19-March	4-May
Visalia, CA	2	19-March	4-May
Bakersfield, CA	3	19-March	4-May
Fresno-Madera-Hanford, CA	4	19-March	4-May
Sacramento-Roseville, CA	5	19-March	4-May
San Diego-Chula Vista-Carlsbad, CA	6	19-March	4-May
Phoenix-Mesa, AZ	7	30-March	30-April
San Jose-San Francisco-Oakland, CA	8	19-March	4-May
Las Vegas-Henderson, NV	9	1-April	30-April
Denver-Aurora, CO	10	26-March	26-April
Salt Lake City-Provo-Orem, UT	11	30-March	13-April
New York-Newark, NY-NY-CT-PA <sup>a</sup>	12	22-March	15-May
Redding-Red Bluff, CA	13	19-March	4-May
Houston-The Woodlands, TX	14	2-April	20-April
El Centro, CA	15	19-March	4-May
Chicago-Naperville, IL-IN-WI <sup>a</sup>	16	23-March	1-May
El Paso-Las Cruces, TX-NM	17	2-April	15-May
Chico, CA	18	19-March	4-May
Fort Collins, CO	19	26-March	26-April
Washington-Baltimore-Arlington, DC-MD-VA-WV-PA <sup>a</sup>	20	30-March	15-May
Dallas-Fort Worth, TX-OK	21	2-April	20-April
Sheboygan, WI	22	24-April	26-May
Philadelphia-Reading-Camden, PA-NJ-DE-MD <sup>a</sup>	23	30-March	15-May
Milwaukee-Racine-Waukesha, WI	24	24-April	26-May
Hartford-East Hartford, CT	25	23-March	20-May

<sup>a</sup>Dates reflect the period that is the longest for any given state in the region.

shows that the COVID-19 lockdown led to  $-28\%$  to  $-48\%$  reductions in on-road NO<sub>x</sub> emissions in the fuel-based inventory. The regions with the two smallest changes in the on-road NO<sub>x</sub> inventory are Atlanta ( $-28\%$ ) and San Joaquin Valley ( $-33\%$ ). Atlanta and the San Joaquin Valley exhibited the smallest drops in

**Table 2**

*Reductions in On-Road NO<sub>x</sub> Emissions and TropNO<sub>2</sub> Between 15 March to 30 April and 1 January to 29 February Derived Using Double Differencing Technique*

City	2019ΔNO <sub>x</sub>	2020ΔNO <sub>x</sub>	Seasonality removed on-road NO <sub>x</sub> emissions changes (%) (2020ΔNO <sub>x</sub> - 2019ΔNO <sub>x</sub> )	2019ΔNO <sub>2</sub>	2020ΔNO <sub>2</sub>	Seasonality removed TropNO <sub>2</sub> reductions (%) (2020ΔtropNO <sub>2</sub> - 2019ΔtropNO <sub>2</sub> )
	(%)	(%)	(%)	(%)	(%)	(%)
Atlanta	10.41	-17.70	-28.11	-22.67	-44.14	-21.47
San Francisco	10.54	-33.95	-44.49	-23.79	-48.18	-24.39
San Joaquin Valley	14.27	-18.39	-32.66	-27.30	-44.62	-17.32
New York City	11.04	-36.87	-47.91	-6.07	-34.05	-27.98
Los Angeles	10.57	-25.10	-35.67	-37.90	-59.68	-21.78

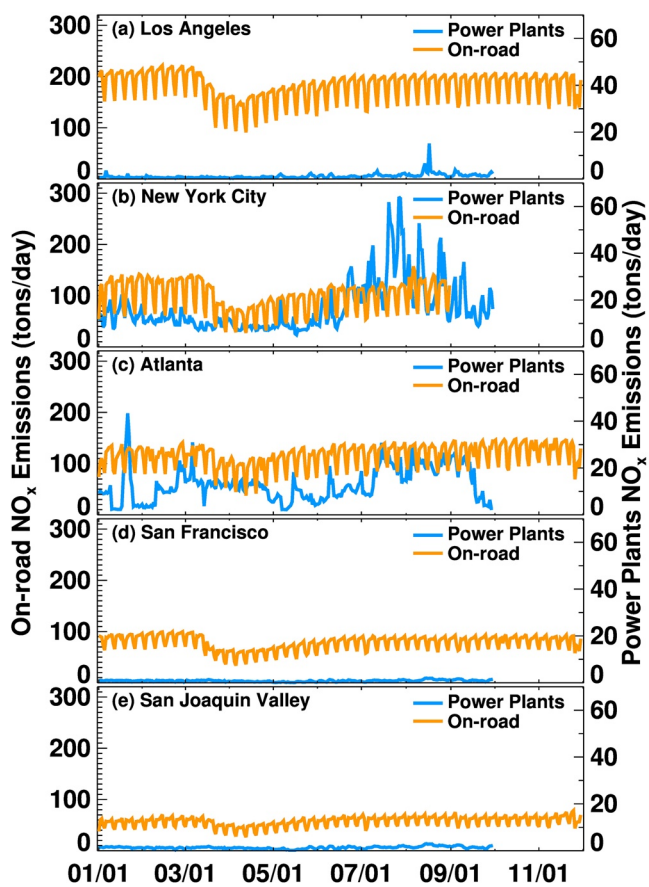


**Figure 3.** Time series of daily on-road and power plant  $\text{NO}_x$  emissions for different cities from January to November 2020. Note that the on-road  $\text{NO}_x$  emissions time series ends on 31 August for New York City because the traffic count data are not available for September to November.

not show a noticeable drop-off in emissions during the most stringent months of the COVID-19 lockdown (i.e., March 15 to April 30) like for on-road transportation. Next, we explore more quantitatively the extent to which on-road  $\text{NO}_x$  emissions are correlated with  $\text{tropNO}_2$  satellite columns.

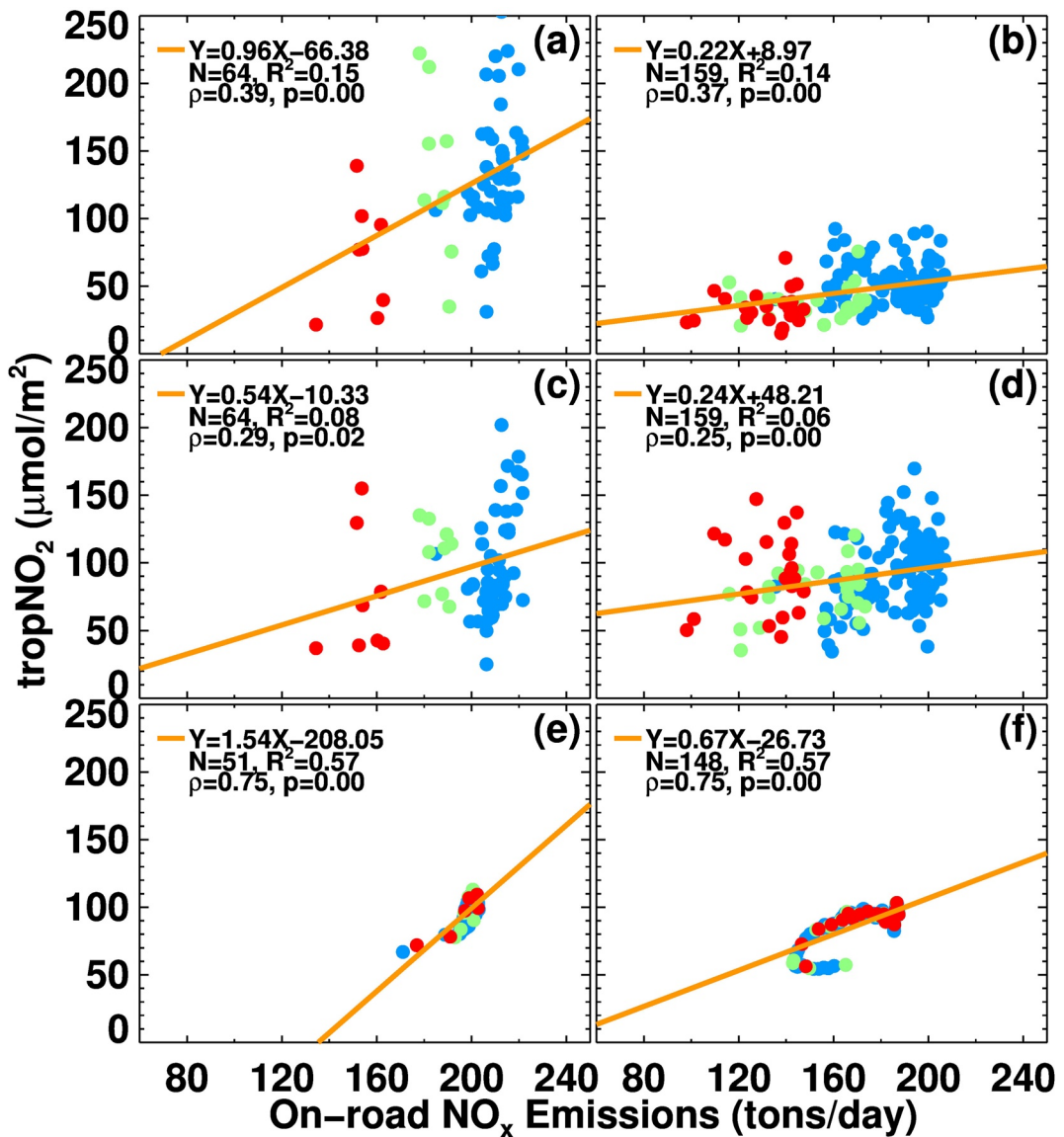
### 3.3. Correlation between On-Road $\text{NO}_x$ Emissions and $\text{tropNO}_2$

Given the knowledge of changes in on-road emissions in the five cities due to lockdown, we wanted to examine if  $\text{tropNO}_2$  shows similar behavior by exhibiting a linear relationship, and if so demonstrate that the period for which the lowest  $\text{NO}_x$  emissions were observed in traffic data also corresponds to the lowest observed  $\text{tropNO}_2$  data. Additionally, we wanted to check if the post-lockdown recovery in traffic emissions is reflected in  $\text{tropNO}_2$  data. We first examined the direct relationship between daily  $\text{tropNO}_2$  and daily on-road  $\text{NO}_x$  emissions for the five locations; but only the analysis for Los Angeles is shown in Figure 4 for illustration purpose; data from other cities showed similar behavior. The  $\text{tropNO}_2$  and  $\text{NO}_x$  emissions (tons/day) for January and February 2020, representing the BAU, and for March through November 2020 are shown in Figures 4a and 4b, respectively. The coincident observations of  $\text{tropNO}_2$  amount sampled in the predominant wind direction are linearly correlated with on-road  $\text{NO}_x$  emissions but the correlation is weak ( $r = 0.39$ ). The traffic emissions fall into three clusters corresponding to emissions on Sundays ( $\sim 150$  tons/day), Saturdays ( $\sim 180$  tons/day), and weekdays ( $\sim 199$  tons/day) with minimal variability in each cluster, whereas  $\text{tropNO}_2$  amount varies between 50 and 225  $\mu\text{moles/m}^2$ .

heavy-duty truck traffic during the lockdown period (defined as March 15 to April 30). Passenger traffic fell the least in the San Joaquin Valley versus the other four cities. New York City exhibited the largest on-road  $\text{NO}_x$  decreases ( $-48\%$ ), which was due to the largest drop in heavy-duty truck traffic across the five regions. As shown in Table 2, the largest reductions in  $\text{tropNO}_2$  were observed for New York City ( $-28\%$ ) and the smallest reductions were observed for San Joaquin Valley ( $-17\%$ ) and Atlanta ( $-21\%$ ). This is generally consistent with the expected changes in the on-road emissions inventory.

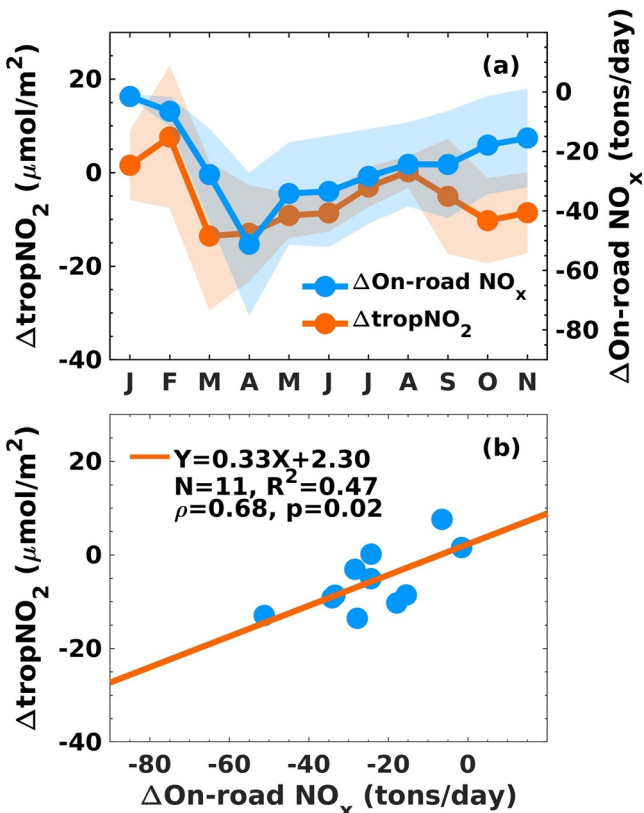
Goldberg et al. (2020) reported  $\text{tropNO}_2$  reductions of 20.2%, 18%, and 39% for Atlanta, New York, and Los Angeles, respectively, and their analysis is also for a lockdown period spanning 15 March to 30 April, 2020. Our analysis shows that  $\text{tropNO}_2$  reductions for these three cities are 21%, 17%, and 22%. Though the methodology used to remove the seasonality is different, the reductions in  $\text{tropNO}_2$  from our analysis and that of Goldberg et al. (2020) are similar, with Los Angeles showing the biggest drop in  $\text{tropNO}_2$  due to lockdown measures. This elucidates the need to account for differences in seasonality and meteorology when analyzing the data for COVID-19 trends (Gkatzelis et al., 2021).

Figure 3 shows the time series of on-road mobile (cars and trucks combined) and power plant  $\text{NO}_x$  emissions for the five different cities/regions in the US from January to November 2020; the exception is New York City for which the time series ends on 31 August due to the nonavailability of traffic data. There are a couple of key points illustrated by Figure 3. First, note the differential scaling of the left and right axes indicating that on-road  $\text{NO}_x$  emissions dominate over power plants across these five regions, except for New York City where power plant emissions are about half of the on-road  $\text{NO}_x$  in summer months. It is noteworthy that there was a jump in power plant emissions toward the end of June, which coincided with the opening of retail establishments on 22 June; the power plant emissions in New York City are higher in summer than in winter, associated with increased demand for air conditioning. Second, the power plant  $\text{NO}_x$  emission trends are distinct from the on-road emission trends and do



**Figure 4.** Correlation between daily tropNO<sub>2</sub> and daily on-road NO<sub>x</sub> emissions for Los Angeles, CA. (a), (c), and (e) For pre-lockdown (January and February) and (b), (d), and (f) for lockdown and post lockdown period (March through end of November). (a) and (b) are daily tropNO<sub>2</sub>, (c) and (d) are daily tropNO<sub>2</sub> normalized to account for meteorology, (e) and (f) are 28-day rolling mean normalized daily tropNO<sub>2</sub>. Red color is for data gathered on Sundays, green color is for data gathered on Saturdays, and blue color is for data gathered on weekdays.

The variability in tropNO<sub>2</sub> can be attributed to different reasons. First, the day-to-day variability in cloud cover can lead to gaps in data. We used the recommended quality flag threshold of 0.75 to screen out the data that have potential contamination from clouds but this strict screening reduces the number of retrievals for a given location. Second, there is also a variability in the background NO<sub>2</sub> contribution to the tropospheric NO<sub>2</sub> column due to which tropNO<sub>2</sub> does not correlate well with NO<sub>x</sub> emissions from sources on the ground. We analyzed the background NO<sub>2</sub> signal in the tropospheric column amount for TROPOMI for 2019 and 2020 using Silvern et al. (2019) method and found it to be higher due to the longer winter-time lifetime (lower temperature, weak photolysis, stronger wind dispersion, and less wet scavenging) and lower in the summer with monthly mean values ranging between 15 and 20 μmoles/m<sup>2</sup> (Figure S3). Sources of background NO<sub>2</sub> are soil emissions of NO<sub>x</sub>, which are amplified after precipitation events, lightning produced NO<sub>x</sub>, and chemical decomposition of peroxyacetyl and alkyl nitrates. Transport of NO<sub>2</sub> from rural areas can also enhance tropNO<sub>2</sub> values that may not correlate well with NO<sub>x</sub> emissions from sources on



**Figure 5.** Trends in on-road monthly mean  $\text{NO}_x$  emissions (tons/day) and  $\text{tropNO}_2$  ( $\mu\text{moles/m}^2$ ) between 2019 and 2020 averaged for the five analysis cities. (a) Average monthly mean differences for the five cities from January to November. (b) Correlation between five-city average changes in on-road monthly mean  $\text{NO}_x$  emissions and changes in five-city average monthly mean  $\text{tropNO}_2$ .

the ground. Third, wind speed and direction influence the mean tropospheric  $\text{NO}_2$  computed for the Los Angeles basin because if the wind speed is high,  $\text{NO}_2$  is dispersed and transported away from the city and if wind speed is low,  $\text{NO}_2$  accumulates in the city. Any variability associated with background  $\text{NO}_2$  is detected by TROPOMI and accounted for in the column  $\text{NO}_2$  amount, but this has no relation to the  $\text{NO}_x$  emissions from on-road sources on the ground. We did account for the effects of wind in our matchups by sampling the data in the downwind direction but higher wind speeds dilute the  $\text{NO}_2$  concentrations observed by TROPOMI (Figure S4).

Outlier values of  $\text{tropNO}_2$  are between 20 and 30  $\mu\text{moles/m}^2$  even when on-road emissions are high indicating TROPOMI retrievals that are either sampled after pollutants are washed out of the atmosphere due to rain or on days when wind speeds are unusually high. Retrievals can also be noisy and have errors associated with air mass factors and a priori profiles. Parker et al. (2020) report that the Los Angeles basin was unusually wet in 2020, especially during the late March and early April 2020. Other researchers who correlated daily surface observations of  $\text{NO}_2$  and TROPOMI  $\text{tropNO}_2$  for 35 different stations in Europe reported similar findings and they found that correlation improved after averaging the data to monthly time scales (Cersosimo et al., 2020; Goldberg et al., 2021; Ialongo et al., 2020). The comparison for the lockdown and post-lockdown period of March through November is shown in Figure 4b; the correlation remains the same ( $r = 0.39$ ) but the one interesting feature is that the  $\text{tropNO}_2$  and on-road emissions are very small during the lockdown compared to the pre-lockdown. Daily  $\text{NO}_x$  emissions on many days are between 100 and 150 tons after 14 March; prior to that, the region was not under stay-at-home orders. The  $\text{tropNO}_2$  never goes above 200  $\mu\text{moles/m}^2$  for this period. Compared to the pre-lockdown period, the on-road  $\text{NO}_x$  emissions and  $\text{tropNO}_2$  values shifted to lower values within each cluster (shown in blue for weekdays, green for Saturdays, and red for Sundays). During the lockdown, one would anticipate that there would not be any difference between weekday and weekend emissions but the difference is stark and is reflected in  $\text{tropNO}_2$  data as well.

We normalized daily  $\text{tropNO}_2$  data to account for meteorological and observational differences from day-to-day using Goldberg et al. (2020) technique as shown in Figures 4c and 4d. Despite normalization, the correlation between daily  $\text{NO}_x$  emissions and  $\text{tropNO}_2$  data did not improve. However, when the normalized data are smoothed with 28-day rolling mean values, the correlation improved with a correlation coefficient of 0.75 for both the pre-lockdown and the lockdown/post-lockdown periods (Figures 4e and 4f). This is consistent with other studies involving satellite  $\text{tropNO}_2$  data where 28-day rolling means or weekly averaging was carried out to minimize noise and data gaps (Goldberg et al., 2021; Misra et al., 2021).

To correlate the changes in on-road  $\text{NO}_x$  emissions with changes in  $\text{tropNO}_2$  between 2019 and 2020 for each of the five regions in this study, we averaged daily  $\text{NO}_x$  emission values and  $\text{tropNO}_2$  values for each month (January to November) and created an average value of all the five regions combined for each month. Figure 5a shows the monthly mean trend plot of  $\Delta \text{NO}_x$  and  $\Delta \text{tropNO}_2$  for January to November; on-road  $\text{NO}_x$  emissions and  $\text{tropNO}_2$  dropped steadily and hit the lowest values in March and April, consistent with the lockdown measures. The recovery began in May and continued to November for on-road  $\text{NO}_x$  emissions but did not completely recover to the pre-lockdown levels. However, the  $\Delta \text{tropNO}_2$  trend plot shows recovery up to August and then begins to show a decline from September to November. This decline in  $\text{tropNO}_2$  is attributed to San Joaquin and San Francisco. Figure 5b shows the correlation of on-road  $\text{NO}_x$  emissions changes ( $\Delta \text{NO}_x$ ) between 2020 and 2019 with the difference in  $\text{tropNO}_2$  amounts between 2020 and 2019 ( $\Delta \text{tropNO}_2$ ). The  $\text{NO}_x$  emissions were lower in 2020 compared to 2019 for all the months and all the cities.

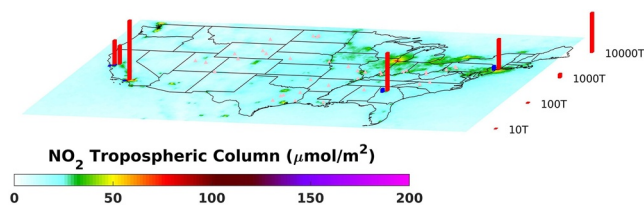


**Figure 6.** tropNO<sub>2</sub> map for second quarter of 2020. The red columns show total on-road NO<sub>x</sub> emissions and the blue columns show NO<sub>x</sub> emissions from power plants nearby these five cities (New York, Atlanta, Los Angeles, San Francisco, and San Joaquin Valley). Power plants with monthly mean NO<sub>x</sub> emissions greater than 1500 tons are also shown in the map as pink dots.

TROPOMI tropNO<sub>2</sub> map as the NO<sub>x</sub> emitted from the power plants mixes and becomes indistinguishable from on-road emissions. Consistent with this analysis, changes in NO<sub>x</sub> emissions between 2020 and 2019 for power plants within 75 km of each of the five analysis cities correlated weakly with changes in tropNO<sub>2</sub> ( $r = 0.35$ ); power plant NO<sub>x</sub> emissions can explain only 12% of the variability seen in tropNO<sub>2</sub> (Figure 7). Also, as can be seen in Figure 7, the daily average changes in power plant emissions between 2020 and 2019 were positive for some plants and negative for some but mostly varied between  $\pm 20$  tons/day.

### 3.4. Correlation Between TropNO<sub>2</sub> and AOD

The premise for the impact of NO<sub>x</sub> emissions reductions on improved air quality due to reduced human activity during the lockdown period depends on how the photochemical processes changed compared to the BAU scenario. The photochemical production of ozone and surface PM<sub>2.5</sub> (particulate mass of particles smaller than 2.5  $\mu\text{m}$  in median diameter) depends not only on NO<sub>x</sub> emissions but also on VOCs and their ratio (Baidar et al., 2015; Parker et al., 2020; McDonald, Gouw, et al., 2018; Qin et al., 2021). Most analyses of the impact of COVID-19 lockdowns on air quality using satellite data have focused on TROPOMI NO<sub>2</sub> and attributed the reductions of NO<sub>x</sub> emissions to improved air quality; the reductions in VOC emissions are largely unknown, especially from nonvehicular sources. Atmospheric formation of nitrate and organic aerosols is driven by NO<sub>x</sub>, VOCs, and ammonia emissions and if the photochemical processes are in a NO<sub>x</sub> limited or VOC limited regime. To analyze the AOD data for indications of reduced aerosol formation due to reduced NO<sub>x</sub> emissions, one complicated factor is the transport of smoke aerosols from upwind regions and how the transported signal can be removed from the AOD data. To address this issue, we tested the hypothesis that the AOD/tropNO<sub>2</sub> ratio is small when pollution sources are local and high when nonlocal sources bring transported aerosols into the domain. We calculated the weekly correlation between AOD and tropNO<sub>2</sub> and obtained the slope for each week over one year in 2019 and 2020, to document the changes in slope as a function of time during the year (Figures 8a–8c); In Figures 8a and 8b, we show an example of how slopes are derived using the scatter plot between VIIRS AOD and TROPOMI tropNO<sub>2</sub> for one week in September 2019 and in 2020. For 2019, when the fire season was not a major contributing factor to aerosol concentrations, the slopes are small in the winter months and slowly increase toward the summer (Figure 8c). This is consistent with the knowledge that ammonium nitrate formation peaks in the summer due to the availability of ammonia from increased agricultural activity and higher volatility associated with higher temperatures (Schiferl et al., 2014).

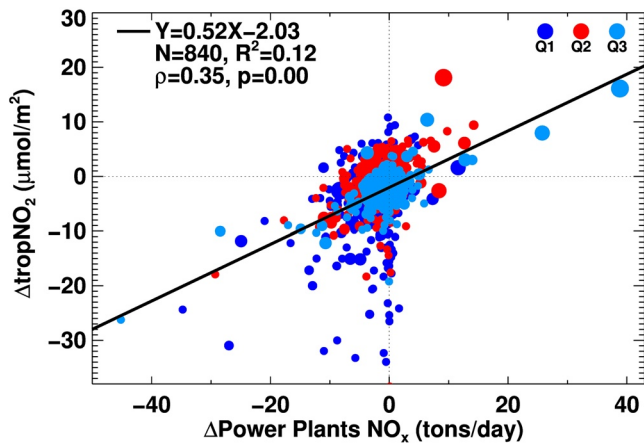


**Figure 7.** Correlation of monthly mean tropNO<sub>2</sub> changes between 2020 and 2019 with changes in power plant monthly mean NO<sub>x</sub> emissions. The size of the circle indicates the magnitude of total monthly emissions (high, medium, and low) of individual power plant. To obtain monthly means, daily total NO<sub>x</sub> emissions were added and divided by the number of days in a month to get average values in units of tons/day.

The positive linear correlation ( $r = 0.68$ ) suggests that TROPOMI tropNO<sub>2</sub> observations captured the changes in on-road NO<sub>x</sub> emissions and can be used to study the changes in NO<sub>x</sub> emissions due to traffic elsewhere in the US where there are no observations from the ground.

Even though traffic emissions are the dominant source for NO<sub>x</sub>, there are power plants near the cities emitting NO<sub>x</sub> continuously and unlike traffic emissions they do not exhibit a weekday/weekend cycle. Figure 6 shows a map of tropNO<sub>2</sub> for the second quarter in 2020 (April/May/June) with on-road NO<sub>x</sub> emissions and power plant NO<sub>x</sub> emissions for each of the five analysis cities as stacks. The locations of power plants in other parts of the country are circled in pink, indicating that these power plants emit greater than 1,500 tons in a given quarter; power plants with lower monthly NO<sub>x</sub> emissions ( $< 1,500$  tons) are not shown on the map. It is difficult to isolate the NO<sub>2</sub> plumes from power plants in urban areas in the

TROPOMI tropNO<sub>2</sub> map as the NO<sub>x</sub> emitted from the power plants mixes and becomes indistinguishable from on-road emissions. Consistent with this analysis, changes in NO<sub>x</sub> emissions between 2020 and 2019 for power plants within 75 km of each of the five analysis cities correlated weakly with changes in tropNO<sub>2</sub> ( $r = 0.35$ ); power plant NO<sub>x</sub> emissions can explain only 12% of the variability seen in tropNO<sub>2</sub> (Figure 7). Also, as can be seen in Figure 7, the daily average changes in power plant emissions between 2020 and 2019 were positive for some plants and negative for some but mostly varied between  $\pm 20$  tons/day.

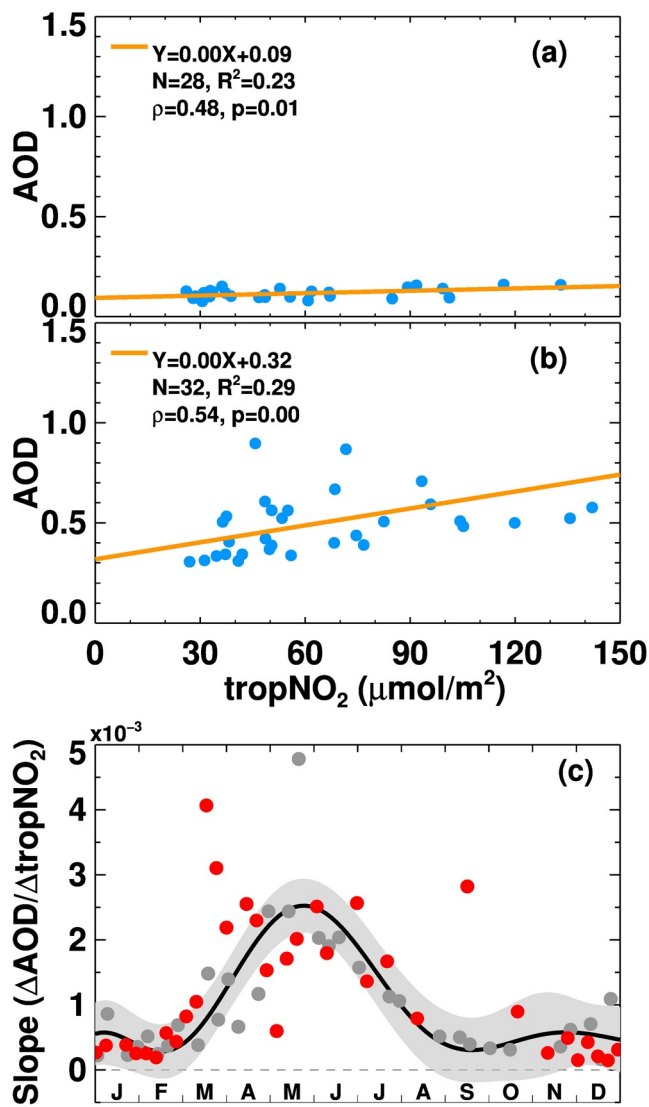


**Figure 8.** (a) Example correlation of VIIRS AOD and TROPOMI tropNO<sub>2</sub> during one week, September 15–21, 2019, (b) Same for September 13–19, 2020, (c) Time series of weekly slope (AOD/tropNO<sub>2</sub>) with data for 2019 in gray color and data for 2020 in red color for Los Angeles, California. The black solid line is the fit to 2019 data indicating seasonal photochemistry. Any data points that depart from the shaded gray region are treated as the period when transported aerosols (e.g., smoke) influenced the air mass over Los Angeles.

monthly scales and even on weekly scales, to the extent that weekday/weekend cycles are noticeable. When using the TROPOMI tropNO<sub>2</sub> data, we wanted to establish that it not only shows the reductions/drop in tropNO<sub>2</sub> due to reductions in on-road NO<sub>x</sub> emissions but that the trend during the post-lockdown recovery phase can be detected as well.

The spatial and temporal analysis, relating indicators of human activity during and prior to the COVID-19 lockdown to air quality conditions, shows that while power plant emission changes were not drastic compared to on-road emissions, the on-road emissions in the five analysis cities dropped coinciding with the start date and the duration of the lockdown. The changes in on-road NO<sub>x</sub> emissions correlated with tropNO<sub>2</sub> changes for these five locations, giving confidence to use tropNO<sub>2</sub> data in other parts of the CONUS, and to draw conclusions about relating changes in tropNO<sub>2</sub> to economic activity changes. We found that the

ranged between 30 and 120  $\mu\text{moles}/\text{m}^2$ , whereas AOD values in 2020 were much higher (between 0.2 and 0.9) compared to values in 2019 (between 0.1 and 0.2). The AOD values in the US typically range between 0 and 1, with higher AODs typically observed in the presence of biomass burning smoke or dust storms. Given this knowledge that slopes are higher when transported aerosol is involved, we were able to filter the AOD data. The filtered data will be used in a future study to analyze trends in AOD due to NO<sub>x</sub> emissions reductions.

### 3.5. Correlation of TropNO<sub>2</sub> and Unemployment Rate

Because of the lockdown measures and work from home policies for majority of the workplaces in the US, the service industry has suffered and the unemployment rate has risen. The US unemployment rate increased from about 4.4% in March to 14.7% in April during the first phase of lockdowns. The unemployment rate nationwide improved as lockdowns were lifted but certain parts of the country continued to experience a very high unemployment rate throughout 2020 (Figure 9). Among the employed, 28% of employees continued to work from home as of November indicating that below normal NO<sub>x</sub> emissions data are to be expected. The correlation between unemployment rate and tropNO<sub>2</sub> for metropolitan areas with a pre-pandemic civilian labor force greater than 2 million is negative for the second and third quarters (the regression line shown in Figure 9 is for second quarter data). The unemployment rate combined with telework policies have contributed to reduced NO<sub>x</sub> emissions and thus lower tropNO<sub>2</sub> values across the US. This is similar to the positive correlation between Gross Domestic Product and tropNO<sub>2</sub> reported by Keller et al. (2020). For reasons unknown, cities such as Phoenix, AZ, Minneapolis, MN, Dallas and Houston, TX, and Chicago, IL showed no change or a slight increase in tropNO<sub>2</sub> in 2020 compared to 2019 though unemployment rate in 2020 was much higher compared to 2019. Keller et al. (2020) do not report these outliers because their analysis is for all developing countries around the world and is not granular at the city level like our analysis.

## 4. Discussion

The TROPOMI tropNO<sub>2</sub> data captures the day-to-day variability in tropospheric NO<sub>2</sub> concentrations but due to cloud cover, varying background tropNO<sub>2</sub>, and uncertainties associated with assumptions such as a priori profile and lower sensitivity to near surface NO<sub>2</sub>, on certain days the tropNO<sub>2</sub> retrievals do not adequately represent the changes in near surface NO<sub>2</sub> (Cersosimo et al., 2020; Goldberg et al., 2021; Ialongo et al., 2020).

The tropospheric NO<sub>2</sub> variability is very well captured; however, on

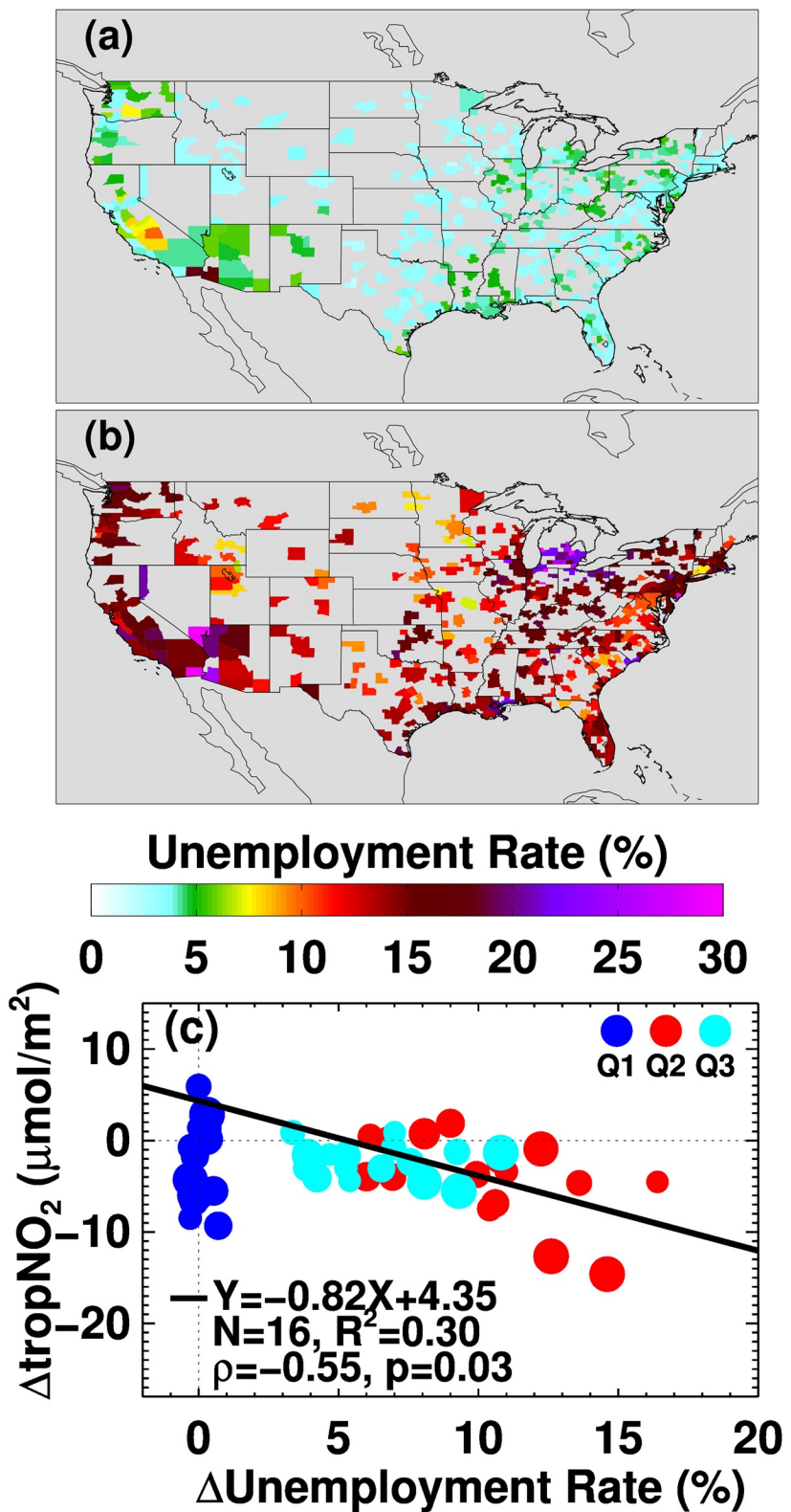


Figure 9.

weekday-weekend differences were pronounced in on-road emissions and tropNO<sub>2</sub> data, and the lowest values of on-road NO<sub>x</sub> occurred on weekends even during the lockdown periods. The unemployment rate and its increase during the lockdown and post lockdown period appears to also be a good proxy for economic activity and is correlated well with the decrease in tropNO<sub>2</sub>. At the height of the lockdown in the second quarter of 2020, the unemployment rate increase was as high as 17% in populated metropolitan areas; even at the end of the third quarter of 2020, the unemployment rate increase was ~10%. The first quarter unemployment rate was constant at ~5% and did not vary; it showed no relationship to tropNO<sub>2</sub> as expected because the impacts due to the lockdown did not affect the unemployment rate until the second quarter.

The satellite data must be analyzed by considering various quality flags and understanding the limitations of the algorithm. It is likely that using the quality flag  $>0.75$  for TROPOMI tropNO<sub>2</sub> was conservative, but the extremely low daily tropNO<sub>2</sub> values on certain days even when on-road NO<sub>x</sub> emissions were high is indicative that the TROPOMI data are more interpretable when averaged to weekly or monthly time scales. For tropNO<sub>2</sub> retrievals that have quality flags between 0.5 and 0.75 suggesting cloud contamination, in future work, we will look at the coincident high-resolution (750 m) VIIRS cloud mask product to analyze TROPOMI flags for cloud contamination. This will help improve our analysis using the daily tropNO<sub>2</sub> retrievals by either including more retrievals or removing some retrievals from the matching with on-road NO<sub>x</sub> emissions data.

## 5. Conclusions

It has already been established by numerous research studies that reduced traffic (on-road) and industrial emissions led to improved air quality during the COVID-19 lockdown measures implemented by various countries across the globe. However, most studies used mobility data as a proxy for reduced human activity to interpret satellite observations of tropNO<sub>2</sub> but did not directly relate the reduced on-road emissions with reduced air quality observations. Here, for the first time, we directly correlate on-road NO<sub>x</sub> emissions data to TROPOMI tropNO<sub>2</sub> in four urban and one rural area in the US. For this, we used TROPOMI tropNO<sub>2</sub>, VIIRS AOD, on-road NO<sub>x</sub> emissions, and unemployment rates to develop a comprehensive analysis for 2019 and 2020. Where needed, we conducted rotated wind analyses and normalization to account for meteorological influences to sample correctly and match the on-road NO<sub>x</sub> emissions with tropNO<sub>2</sub> data. We also developed a novel way of deseasonalizing tropNO<sub>2</sub> data, and used changes in unemployment rate data as an indicator for economic activity.

Our analysis of reductions in on-road NO<sub>x</sub> emissions from light- and heavy-duty vehicles derived from fuel sales data showed a reduction from 9% to 19% between February and March 2020. When lockdown measures were the most stringent, at the onset of the lockdown period in the middle of March 2020 in most of the US and between March and April 2020, the on-road NO<sub>x</sub> emissions dropped further by 8%–31%. These precipitous drops in NO<sub>x</sub> emissions correlated well with tropNO<sub>2</sub>. Furthermore, the changes in tropNO<sub>2</sub> across the continental US between 2020 and 2019 correlated well with changes in the on-road NO<sub>x</sub> emissions ( $r = 0.68$ ) but correlated weakly with changes in emissions from power plants ( $r = 0.35$ ). These findings confirm the known fact that power plants are no longer a major source of NO<sub>2</sub> in urban areas of the US. As the US entered a post-pandemic phase between May and November 2020, the increased mobility resulted in increased NO<sub>x</sub> emissions nearly returning to the pre-lockdown phase but not entirely back to 100%. Though the lockdown in most of the US ended by May, the on-road NO<sub>x</sub> emissions did not bounce back to near normal values until August for Atlanta; for San Joaquin Valley, Los Angeles, and San Francisco, the on-road NO<sub>x</sub> emissions continued to be 20% below normal even in November. These changes are reflected in the tropNO<sub>2</sub> data, except for San Francisco and San Joaquin Valley, where the tropNO<sub>2</sub> diverged from on-road NO<sub>x</sub> emissions trends, which needs further inquiry. The positive linear correlation between on-road NO<sub>x</sub> emissions and TROPOMI tropNO<sub>2</sub> ( $r = 0.75$ ) suggests that satellite tropospheric column observations of

**Figure 9.** The impact of COVID-19 lockdown on the unemployment rate in metropolitan areas and tropNO<sub>2</sub>. (a) Unemployment rate in April 2019, (b) Unemployment rate in April 2020, and (c) Correlation between increase in unemployment between 2019 and 2020 and tropNO<sub>2</sub> changes. Only data for metropolitan areas where the civilian labor force in 2019 was greater than 2 million are shown in the correlation plot. In the first quarter (Q01), unemployment changes are close to zero as pandemic impact did not begin until late March. Strong negative correlation is observed for the second (Q02) and third (Q03) quarters. The solid black line is the fit to the second quarter data.

NO<sub>2</sub> captured the changes in on-road emissions and can be used to study changes in NO<sub>x</sub> emissions due to traffic where ground observations are not available.

The negative correlation between changes in tropNO<sub>2</sub> and increased unemployment rate indicates that with the increased unemployment rate combined with telework policies across the US for nonessential workers, the tropNO<sub>2</sub> values decreased at the rate of 0.8 μmoles/m<sup>2</sup> per unit percentage increase in the unemployment rate.

Across the US, we found positive spatial correlation between S5P TROPOMI tropNO<sub>2</sub> and Suomi NPP VIIRS AOD measurements in urban regions indicating common source sectors for NO<sub>2</sub> and aerosols/aerosol precursors. We developed a new mechanism using the changes in AOD-tropNO<sub>2</sub> slope to screen for fire events influencing aerosol concentrations in urban/industrial regions that can be used to analyze changes in aerosols due to emissions reductions. The COVID-19 pandemic experience has provided the scientific community an opportunity to identify scenarios that can lead to a new normal urban air quality and assess if the new normal can be sustained with novel policies such as increased telework and a shift toward driving electric cars.

#### Acknowledgments

This work is part of a NOAA wide COVID-19 project funded by the Joint Polar Satellite System (JPSS) and the office of Oceanic and Atmospheric Research (OAR) to investigate the impact of lockdown on aerosols and trace gases including greenhouse gases. The authors thank Mitch Goldberg (Chief Scientist of NOAA National Environmental Satellite Data and Information Services), Greg Frost (Program Manager, NOAA Climate Program Office), and Satya Kalluri (Science Advisor to the JPSS program) for securing funds for this work. The authors thank the European Space Agency for the provision of the Sentinel 5 Precursor Tropospheric Monitoring Instrument data. The authors also thank members of the NOAA NESDIS JPSS aerosol calibration and validation team for the routine validation of Suomi National Polar-orbiting Partnership Visible Infrared Imaging Radiometer Suite aerosol optical depth product (Istvan Laszlo, Hongqing Liu, and Hai Zhang) used in our analysis. The authors thank Meng Li (NOAA Cooperative Institute for Research in Environmental Sciences) and Jian He (NOAA Cooperative Institute for Research in Environmental Sciences) for providing the results of WRF-Chem simulations used to help interpret the results shown in Figure 2. Brian McDonald acknowledges the support from NOAA NRDD Project (#19533) - "COVID-19: Near Real-time Emissions Adjustment for Air Quality Forecasting and Long-Term Impact Analyses." Daniel Tong acknowledges the partial support of NOAA Weather Program Office (NA19OAR4590082), and Daniel Goldberg acknowledges the support of NASA RRNES grant #: 80NSSC20K1122. The authors acknowledge the help of Amy Huff (IM Systems Group) in proof reading the manuscript.

#### Disclaimer

The scientific results and conclusions, as well as any views or opinions expressed herein, are those of the author(s) and do not necessarily reflect those of NOAA or the Department of Commerce.

#### Data Availability Statement

The publicly available pixel-level SNPP VIIRS AOD data can be obtained from NOAA CLASS (<https://www.avl.class.noaa.gov>). The pixel-level Sentinel 5P TROPOMI NO<sub>2</sub> data can be obtained at <https://scihub.copernicus.eu/dhus/#/home>. The Level 3 gridded products of TROPOMI NO<sub>2</sub> and VIIRS AOD can be generated by regridding pixel-level data into desired grid resolution by users. The on-road NO<sub>x</sub> emissions data are available at <https://csl.noaa.gov/groups/csl7/measurements/2020covid-aqs/emissions/>.

#### References

Achakulwisut, P., Brauer, M., Hystad, P., & Anenberg, S. C. (2019). Global, national, and urban burdens of paediatric asthma incidence attributable to ambient NO<sub>2</sub> pollution: Estimates from global datasets. *Lancet Planet Health*, 3, 1–4. [https://doi.org/10.1016/S2542-5196\(19\)30046-4](https://doi.org/10.1016/S2542-5196(19)30046-4)

Baidar, S., Hardsty, R. M., Kim, S.-W., Langford, A. O., Oetjen, H., Semff, C. J., et al. (2015). Weakening of the weekend ozone effect over California's South Coast Air Basin: Weekend ozone effect over California. *Geophysical Research Letters*, 42, 9457–9464. <https://doi.org/10.1002/2015GL06419>

Bauwens, M., Compernolle, S., Stavrakou, T., Muller, J.-F., van Gent, J., Eskes, H., et al. (2020). Impact of Coronavirus Outbreak on NO<sub>2</sub> Pollution Assessed Using TROPOMI and OMI Observations. *Geophysical Research Letters*, 47, e2020GL087978. <https://doi.org/10.1029/2020GL087978>

Bishop, G. A., & Stedman, D. H. (2014). The recession of 2008 and its impact on light-duty vehicle emissions in three western United States cities. *Environmental Science & Technology*, 48, 14822–14827. <https://doi.org/10.1021/es5043518>

Cersosimo, A., Serio, C., & Masiello, G. (2020). TROPOMI NO<sub>2</sub> Tropospheric Column Data: Regridding to 1 km Grid-Resolution and Assessment of their Consistency with In Situ Surface Observations. *Remote Sensing*, 12, 2212. <https://doi.org/10.3390/rs1214221>

Chan, K. L., Wiegner, M., van Geffen, J., De Smedt, I., Alberti, C., Cheng, Z., et al. (2020). MAX-DOAS measurements of tropospheric NO<sub>2</sub> and HCHO in Munich and the comparison to OMI and TROPOMI satellite observations (2020). *Atmospheric Measurement Techniques*, 13, 4499–4520. <https://doi.org/10.5194/amt-13-4499-2020>

de Gouw, J. A., Parrish, D. D., Frost, G. J., & Trainer, M. (2014). Reduced emissions of CO<sub>2</sub>, NO<sub>x</sub>, and SO<sub>2</sub> from U.S. power plants owing to switch from coal to natural gas with combined cycle technology. *Earth's Future*, 2, 75–82. <https://doi.org/10.1002/2013EF000196>

EPA. (2015). *MOVES2014a (Motor vehicle emission simulator)*, office of transportation and air quality. U.S. Environmental Protection Agency.

Fioletov, V. E., McLinden, C. A., Krotkov, N., & Li, C. (2015). Lifetimes and emissions of SO<sub>2</sub> from point sources estimated from OMI. *Geophysical Research Letters*, 42, 1969–1976. <https://doi.org/10.1002/2015GL063148>

Gkatzelis, G. I., J. B. Gilman, S. S. Brown, H. Eskes, A. R. Gomes, A. C. Lange, et al. (2021). The Global Impacts of COVID-19 Lockdowns on Urban Air Pollution: A Review. *Elementa: Science of Anthropocene*, 9 (1). 00176. <https://doi.org/10.1525/elementa.2021.00176>

Goldberg, D. L., Anenberg, S. C., Griffin, D., McLinden, C. A., Lu, Z., & Streets, D. G. (2020). Disentangling the impact of the COVID-19 lockdowns on urban NO<sub>2</sub> from natural variability. *Geophysical Research Letters*, 47, e2020GL089269. <https://doi.org/10.1029/2020GL089269>

Goldberg, D. L., Anenberg, S. C., Kerr, G. H., Mohegh, A., Lu, Z., & Streets, D. G. (2021). TROPOMI NO<sub>2</sub> in the United States: A detailed look at the annual averages, weekly cycles, effects of temperature, and correlation with surface NO<sub>2</sub> concentrations. *Earth's Future*, 9, e2020EF001665. <https://doi.org/10.1029/2020ef001665>

Goldberg, D. L., Lu, Z., Streets, D. G., de Foy, B., Griffin, D., McLinden, C. A., et al. (2019). Enhanced capabilities of TROPOMI NO<sub>2</sub>: Estimating NO<sub>x</sub> from North American 2 cities and power plants. *Environmental Science & Technology*, 53(21), 12594–12601. <https://doi.org/10.1021/acs.est.9b04488>

Harkins, C., McDonald, B. C., Henze, D. K., & Wiedinmyer, C. (2021). A fuel-based method for updating mobile source emissions during the COVID-19 pandemic. *Environmental Research Letters*, 16, 065018. <https://doi.org/10.1088/1748-9326/ac0660>

Hassler, B., McDonald, B. C., Frost, G. J., Borbon, A., Carslaw, D. C., Civerolo, K., et al. (2016). Analysis of long-term observations of NO<sub>x</sub> and CO in megacities and application to constraining emissions inventories. *Geophysical Research Letters*, 43, 9920–9930. <https://doi.org/10.1002/2016gl069894>

Hersbach, H., Bell, B., Berrisford, P., Hirahara, S., Horanyi, A., Munoz-Sabater, J., et al. (2020). The ERA5 global reanalysis. *Quarterly Journal of the Royal Meteorological Society*, 146, 1999–2049. <https://doi.org/10.1002/qj.3803>

Hoesly, R. M., Smith, S. J., Feng, L., Klimont, Z., Janssens-Maenhout, G., Pitkanen, T., et al. (2018). Historical (1750–2014) anthropogenic emissions of reactive gases and aerosols from the Community Emissions Data System (CEDS). *Geoscientific Model Development*, 11, 369–408. <https://doi.org/10.5194/gmd-11-369-2018>

Huang, J., Kondragunta, S., Laszlo, I., Liu, H., Remer, L. A., Zhang, H., et al. (2016). Validation and expected error estimation of Suomi-NPP VIIRS aerosol optical thickness and Ångström exponent with AERONET. *Journal of Geophysical Research - D: Atmospheres*, 121, 7139–7160. <https://doi.org/10.1002/2016JD024834>

Ialongo, I., Virta, H., Eskes, H., Hovila, J., & Douros, J. (2020). Comparison of TROPOMI/Sentinel 5 Precursor NO<sub>2</sub> observations with ground-based measurements in Helsinki. *Atmos. Measurement Techniques*, 13, 205–218. <https://doi.org/10.5194/amt-2019-329>

Jiang, Z., McDonald, B. C., Worden, H., Worden, J. R., Miyazaki, K., Qu, Z., et al. (2018). Unexpected slowdown of US pollutant emission reduction in the past decade. *Proceedings of the National Academy of Sciences of the United States of America*, 115, 5099–5104. <https://doi.org/10.1073/pnas.1801191115>

Judd, L. M., Al-Saadi, J. A., Szykman, J. J., Valin, L. C., Janz, S. J., Kowalewski, M. G., et al. (2020). Evaluating Sentinel-5P TROPOMI tropospheric NO<sub>2</sub> column densities with airborne and Pandora spectrometers near New York City and Long Island Sound. *Atmospheric Measurement Techniques*, 13, 6113–6140. <https://doi.org/10.5194/amt-13-6113-2020>

Keller, C. A., Evans, M. J., Knowland, K. E., Hasenkopf, C. A., Modekurty, S., Lucchesi, R. A., et al. (2020). Global Impact of COVID-19 Restrictions on the Surface Concentrations of Nitrogen Dioxide and Ozone. *Atmospheric Chemistry and Physics Discussions*, 21. [preprint] in review. <https://doi.org/10.5194/acp-2020-685>

Kim, S.-W., McDonald, B. C., Baidar, S., Brown, S. S., Dube, B., Ferrare, R. A., et al. (2016). Modeling the weekly cycle of NO<sub>x</sub> and CO emissions and their impacts on O<sub>3</sub> in the Los Angeles-South Coast Air Basin during the CalNex 2010 field campaign. *Journal of Geophysical Research - D: Atmospheres*, 121, 1340–1360. <https://doi.org/10.1002/2015JD024292>

Kondragunta, S., Crisp, D., & Zehner, C. (2020). Disseminating scientific results in the age of rapid communication. *Eos*, 101. Published on 20 October 20. <https://doi.org/10.1029/2020EO150710>

Kroll, J. H., Heald, C. L., Cappa, C. D., Farmer, D. K., Fry, J. L., Murphy, J. G., et al. (2020). The complex chemical effects of COVID-19 shutdowns on air quality. *Nature Chemistry*, 12, 777–779. <https://doi.org/10.1038/s41557-020-0535-z>

Lamsal, N. L., Duncan, B. N., Yoshida, Y., Krotkov, N. A., Pickering, K. E., & Streets, D. (2015). U.S. NO<sub>2</sub> trends (2005–2013): EPA Air Quality System (AQS) data versus improved observations from the Ozone Monitoring Instrument (OMI). *Atmospheric Environment*, 100, 130–143. <https://doi.org/10.1016/j.atmosenv.2015.03.055>

Laszlo, I., & Liu, H. (2016). *EPS aerosol optical depth (AOD) algorithm theoretical BasisDocument*, version 3.0.1, June 28, 2016. NOAA NESDIS.

Levy, R. C., Remer, L. A., Mattoo, S., Vermote, E. F., & Kaufman, Y. J. (2007). Second-generation operational algorithm: Retrieval of aerosol properties over land from inversion of Moderate Resolution Imaging Spectroradiometer spectral reflectance. *Journal of Geophysical Research*, 112, D13211. <https://doi.org/10.1029/2006JD007811>

Lin, J.-T., Martin, R. V., Boersma, K. F., Sneep, M., Stammes, P., Spurr, R., et al. (2014). Retrieving tropospheric nitrogen dioxide from the Ozone Monitoring Instrument: Effects of aerosols, surface reflectance anisotropy, and vertical profile of nitrogen dioxide. *Atmospheric Chemistry and Physics*, 14, 1441–1461. <https://doi.org/10.5194/acp-14-1441-2014>

Liu, F., Liu, M., Lin, J., Kong, H., Boersma, K. F., Eskes, H., et al. (2021). Abrupt decline in tropospheric nitrogen dioxide after the outbreak of COVID-19. Paper presented at 101st virtual American Meteorological Association meeting.

Liu, F., Page, A., Strode, S. A., Yoshida, Y., Choi, S., Zheng, B., et al. (2020). Abrupt decline in tropospheric nitrogen dioxide over China after the outbreak of COVID-19. *Science Advances*, 6, 28. eabc2992. <https://doi.org/10.1126/sciadv.abc2992>

Liu, M., J. Lin, H. Kong, K. F. Boersma, H. Eskes, Y. Kanaya, et al. (2020). A new TROPOMI product for tropospheric NO<sub>2</sub> columns over East Asia with explicit aerosol corrections. *Atmospheric Measurement Techniques*, 13, 4247–4259. <https://doi.org/10.5194/amt-13-4247-2020>

Lorente, A., Boersma, K. F., Eskes, H. J., Veenkind, J. P., van Geffen, J. H. G. M., de Zeeuw, H. J., et al. (2019). Quantification of nitrogen oxides emissions from build-up of pollution over Paris with TROPOMI. *Scientific Reports*, 9, 20033. <https://doi.org/10.1038/s41598-019-56428-5>

Mazuca, G. M., Ren, X., Loughner, C. P., Estes, M., Crawford, J. H., Pickering, K. E., et al. (2016). Ozone production and its sensitivity to NO<sub>x</sub> and VOCs: Results from the DISCOVER-AQ field experiment, Houston 2013. *Atmospheric Chemistry and Physics*, 16, 14463–14474. <https://doi.org/10.5194/acp-16-14463-2016>

McDonald, B. C., Dallmann, T. R., Martin, E. W., & Harley, R. A. (2012). Long-term trends in nitrogen oxide emissions from motor vehicles at national, state, and air basin scales. *Journal of Geophysical Research*, 117, D00V18. <https://doi.org/10.1029/2012JD018304>

McDonald, B. C., de Gouw, J. A., Gilman, J. B., Jathar, S. H., McDonald, B. C., & Akherati, A. (2018). Volatile chemical products emerging as largest petrochemical source of urban organic emissions. *Science*, 359, 760–764. <https://doi.org/10.1126/science.aao524>

McDonald, B. C., McBride, Z. C., Martin, E. W., & Harley, R. A. (2014). High-resolution mapping of motor vehicle carbon dioxide emissions. *Journal of Geophysical Research: Atmospheres*, 119, 5283–5298. <https://doi.org/10.1002/2013jd021219>

McDonald, B. C., McKeen, S. A., Cui, Y. Y., Ahmadov, R., Kim, S. W., Frost, G. J., et al. (2018). Modeling ozone in the Eastern U.S. using a fuel-based mobile source emissions inventory. *Environmental Science & Technology*, 52, 7360–7370. <https://doi.org/10.1021/acs.est.8b00778>

Misra, P., Takigawa, M., Khatri, P., Dhaka, S. K., Dimri, A. P., Yamaji, K., et al. (2021). Nitrogen oxides concentration and emission change detection during COVID-19 restrictions in North India. *Scientific Reports*, 11, 9800. <https://doi.org/10.1038/s41598-021-87673-2>

Naeger, A. R., & Murphy, K. (2020). Impact of COVID-19 Containment Measures on Air Pollution in California. *Aerosol and Air Quality Research*, 20. <https://doi.org/10.4209/aaqr.2020.05.0227>

Parker, H. A., Hasheminassab, S., Crounse, J. D., Roehl, C. M., & Wennberg, P. O. (2020). Impacts of traffic reductions associated with COVID-19 on Southern California air quality. *Geophysical Research Letters*, 47, e2020GL090164. <https://doi.org/10.1029/2020GL090164>

Qin, M., Murphy, B. N., Isaacs, K. K., McDonald, B. C., Lu, Q., McKeen, S. A., et al. (2021). Criteria pollutant impacts of volatile chemical products informed by near-field modelling. *Nature Sustainability*, 4, 129–137. <https://doi.org/10.1038/s41893-020-00614-1>

Qu, Z., Jacob, D. J., Silvern, R. F., Shah, V., Campbell, P. C., Valin, L. C., & Murray, L. T. (2021). US COVID-19 shutdown demonstrates importance of background NO<sub>2</sub> in inferring NO<sub>x</sub> emissions from satellite NO<sub>2</sub> observations. *Geophysical Research Letters*, 48, e2021GL092783. <https://doi.org/10.1029/2021GL092783>

Schiferl, L. D., Heald, C. L., Nowak, J. B., Holloway, J. S., Neuman, J. A., Bahreini, R., et al. (2014). An investigation of ammonia and inorganic particulate matter in California during the CalNex campaign. *Journal of Geophysical Research: Atmospheres*, 119, 1883–1902. <https://doi.org/10.1002/2013JD020765>

Silver, B., He, X., Arnold, S., & Spracklen, D. V. (2020). The impact of COVID-19 control measures on air quality in China. *Environmental Research Letters*, 15, 084021. <https://doi.org/10.1088/1748-9326/aba3a2>

Silvern, R. F., Jacob, D. J., Mickley, L. J., Sulprizio, M. P., Travis, K. R., Marais, E. A., et al. (2019). Using satellite observations of tropospheric NO<sub>2</sub> columns to infer long-term trends in US NO<sub>x</sub> emissions: The importance of accounting for the free tropospheric NO<sub>2</sub> background. *Atmospheric Chemistry and Physics*, 19, 8863–8878. <https://doi.org/10.5194/acp-19-8863-2019>

Straka, W., Kondragunta, S., Wei, Z., Zhang, H., Miller, S. D., & Watts, A. (2021). Examining the economic and environmental impacts of COVID-19 using earth observation data. *Remote Sensing*, 13(1), 5.

Tack, F., Merlaud, A., Meir, A. C., Vlemmix, T., Ruhtz, T., Iordache, M.-D., et al. (2019). Intercomparison of four airborne imaging DOAS systems for tropospheric NO<sub>2</sub> mapping—The AROMAPEX campaign. *Atmospheric Measurement Techniques*, 12, 211–236. <https://doi.org/10.5194/amt-12-2110.5194/amt-12-211-2019>

Vadrevu, K. P., Eaturu, A., Biswas, S., Lasko, K., Sahu, S., Garg, J. K., et al. (2020). Spatial and temporal variations of air pollution over 41 cities of India during the COVID-19 lockdown period. *Scientific Reports*, 10, 16574. <https://doi.org/10.1038/s41598-020-72271-5>

van Geffen, J., Eskes, H. J., Boersma, K. F., Maasakkers, J. D., & Veefkind, J. P. (2019). *TROPOMI ATBD of the total and tropospheric NO<sub>2</sub> data products, S5P-KNMI-L2-0005-RP, v1.4.0*.

Zhang, H., & Kondragunta, S. (2021). Daily and hourly surface PM2.5 estimation from satellite AOD. *Earth and Space Science*, 8, e2020EA001599. <https://doi.org/10.1029/2020EA001599>

Zhang, H., Kondragunta, S., Laszlo, I., Liu, H., Remer, L. A., Huang, J., et al. (2016). An enhanced VIIRS aerosol optical thickness (AOT) retrieval algorithm over land using a global surface reflectance ratio database. *Journal of Geophysical Research: Atmospheres*, 121, 10717–10738. <https://doi.org/10.1002/2016JD024859>

Zhang, Q., Pan, Y., He, Y., Walters, W. W., Ni, Q., Liu, X., et al. (2021). Substantial nitrogen oxides emission reduction from China due to COVID-19 and its impact on surface ozone and aerosol pollution. *Science of The Total Environment*, 753. <https://doi.org/10.1016/j.scitotenv.2020.142238>

Zhao, X., Griffin, D., Fioletov, V., McLinden, C., Cede, A., Tiefengraber, M., et al. (2020). Assessment of the quality of TROPOMI high-spatial-resolution NO<sub>2</sub> data products in the Greater Toronto Area. *Atmospheric Measurement Techniques*, 13, 2131–2159. <https://doi.org/10.5194/amt-13-2131-2020>

Zheng, H., Kong, S., Chen, N., Yan, Y., Liu, D., Zhu, B., et al. (2020). Significant changes in the chemical compositions and sources of PM2.5 in Wuhan since the city lockdown as COVID-19. *Science of The Total Environment*, 739.